Journal of Advanced Ceramics
2017, **6**(3): 220–229
https://doi.org/10.1007/s40145-017-0233-5
ISSN 2226-4108
CN 10-1154/TQ

Research Article

Shaped Co^{2+} doped TiO_2 nanocrystals synthesized from nanotubular precursor: Structure and ferromagnetic behavior

M. VRANJEŠ[a], J. KULJANIN JAKOVLJEVIĆ[a], Z. KONSTANTINOVIĆ[b], A. POMAR[c], M. STOILJKOVIĆ[a], M. MITRIĆ[a], T. RADETIĆ[d], Z. ŠAPONJIĆ[a,*]

[a]*Vinča Institute of Nuclear Sciences*, *University of Belgrade*, *P.O. Box 522*, *11001 Belgrade*, *Serbia*
[b]*Center for Solid State Physics and New Materials*, *Institute of Physics Belgrade*, *University of Belgrade*, *Pregrevica 118*, *11080 Belgrade*, *Serbia*
[c]*Institut de Ciència de Materials de Barcelona*, *CSIC*, *Campus UAB*, *08193 Bellaterra*, *Spain*
[d]*Faculty of Technology and Metallurgy*, *University of Belgrade*, *Karnegijeva 4*, *11120 Belgrade*, *Serbia*

Received: January 02, 2017; Revised: April 24, 2017; Accepted: May 31, 2017

Abstract: Co^{2+} doped TiO_2 nanocrystals were synthetized by a hydrothermal treatment procedure applied to precursor dispersion of titania nanotubes and Co^{2+} ions. Mixture of polygonal and prolate spheroid-like nanocrystals was obtained. The results of X-ray diffraction (XRD) analysis showed that resulted nanocrystals retain anatase crystal phase for both dopant concentrations (1.69 and 2.5 at%), but the crystal lattice parameters were affected. Reflection spectra revealed altered optical properties compared to bare TiO_2. Room temperature ferromagnetic ordering with saturation magnetic moment in the range of 0.001–0.002 μ_B/Co was observed for both measured films made of Co^{2+} doped TiO_2 nanocrystals.

Keywords: hydrothermal synthesis; X-ray diffraction (XRD); transmission electron microscopy (TEM); doped TiO_2; magnetic properties

1 Introduction

The ability to control the spin of electrons in addition to their charge in materials such as nanoscale diluted magnetic semiconductors (DMSs) would expand their applications from conventional to spin-based electronic devices. Traditionally, the DMSs refer to a non-magnetic semiconductor material, as a host, in which a few atomic percents of its cations are replaced with transition metal ions. DMSs are mostly based on III–V (GaN, GaP, etc.) or II–VI (ZnS, CdTe) compounds because, among other things, valence of host cations (+3 or +2) matches well that of common magnetic ions. Generally, in these materials, ferromagnetism has been achievable far below room temperature. Typically, they have Curie temperatures below 100 K making them unattractive for practical applications in future devices characterized by simultaneous control of spin and charge of electrons [1]. Recently, oxide (ZnO, TiO_2, SnO_2, In_2O_3)-based DMS materials have attracted considerable attention due to the reports of ferromagnetism at room temperature which open the possibility of their application in emerging field of thin-film magneto-optic and spin-electronic devices [2–12].

The origin of ferromagnetism in oxide DMSs is still subject of controversy and the debate spans from

* Corresponding author.
E-mail: saponjic@vinca.rs

intrinsic ferromagnetism over possible precipitation of magnetic clusters to the formation of secondary magnetic phases [13]. Generally, conventional exchange mechanisms (direct or superexchange interactions) used for explanation of ferromagnetic behavior cannot be applied on oxide DMSs. The reason is the absence of long-range magnetic ordering at applied concentrations of 3d dopants that are far below the percolation threshold associated with nearest-neighbor cation coupling [14]. Numerous studies, experimental and theoretical, suggest that oxygen vacancies, acting as donors who introduce n-type doping in the material, play an important role in the magnetic ordering of oxide DMSs [15–17]. Electrons associated with oxygen vacancy defects tend to form bound magnetic polarons (BMP model), coupling the 3d moments of the dopant ions within their orbits [14].

The differences between the mechanisms of dopant ion incorporations in bulk material and nanocrystals should be taken into account in order to overcome the problems in nanodoping process [18]. More precisely, the problem of so called "self-purifications", according to which the dopant ions are expelled from the nanoparticle core during the crystal growth when synthesis starts from the molecular precursors [19], should be prevailed. We developed hydrothermal synthetic procedure for incorporation of various dopant ions (transition metal ions and rare earth ions) in TiO_2 nanocrystals of various shapes (faceted nanoparticles, prolate nanospheroids) using dispersions of titania nanotubes and dopant ions, as precursors [20–23]. In our previous work, we reported ferromagnetic ordering in faceted Co^{2+} doped TiO_2 nanoparticles synthesized hydrothermally in acidic conditions (pH = 3), by shape transformation of titania nanotubes in the presence of Co^{2+} ions [24]. According to Erwin *et al*. [18], the underlying mechanism that generally controls doping is an initial adsorption of dopant ions on the nanocrystal surface during the growth which is on the other hand controlled by surface morphology and nanocrystal shape. Having that in mind, we exploited the presence of an undercoordinated defect site on the surface of titania nanotubes for an initial adsorption of dopant anions enabling formation of the highly stable central core of the resulting particle, without influence of further growth on doping efficiency. In theory of transformation of nanotubes, it was suggested that the existing TiO_6 octahedra layers served as a seed layer for the epitaxial anatase crystals nucleating and growing along specific directions on the nanotube surface [25,26].

The aim of this work was to hydrothermally synthesize Co^{2+} doped TiO_2 nanocrystals of different shape, and to examine their shape dependent magnetic, structural, and optical properties. The study of shape dependent magnetic properties of prolate spheroid-like and polygonal (faceted) Co^{2+} doped TiO_2 nanocrystals, for the synthesis of which were used, as precursors, weak acidic (pH = 5) dispersions of titania nanotubes and Co^{2+} ions in two different concentrations, is presented for the first time, to the best of our knowledge. Morphologies of the doped nanocrystals and their crystalline structures were studied by transmission electron microscopy (TEM) and X-ray diffraction (XRD) analysis, respectively. The inductively coupled plasma (ICP) emission spectrometry was applied for determination of the amount of Co^{2+} dopant ions incorporated within TiO_2 nanocrystals. The optical characterization of powdered samples of the Co^{2+} doped TiO_2 nanocrystals was carried out by UV–Vis spectroscopy in reflection mode. The superconducting quantum interference device (SQUID) magnetometer was used to study the magnetic properties of films made of Co^{2+} doped TiO_2 nanocrystals.

2 Experimental procedure

All chemicals were reagent grade from Aldrich and used as received. Titania nanotubes were synthetized via hydrothermal method according to Kasuga *et al*. [27], using commercial TiO_2 powder (Degussa) as precursor. The 2 g of TiO_2 powder was dispersed in 50 mL 10 M NaOH and hydrothermally treated for 48 h in a Teflon vessel (Parr acid digestion bomb, total volume 125 mL) under saturated vapor pressure of water at 120 ℃. After autoclaving, the ensuing powder was washed with 1 M HCl and subsequently with distilled water. Separation of powder from the washing solution, after each washing step, was done by centrifugation. The washing procedure was repeated until pH of water achieved 7. The powder was then air dried at 70 ℃.

For the synthesis of Co^{2+} doped TiO_2 nanocrystals, two precursor dispersions of titania nanotubes (125 mg/50 mL each) at pH = 5 containing two different concentrations of $CoCl_2$ (3.11×10^{-4} and 6.23×10^{-4} M) were prepared and stirred for 3 h at room temperature after which the hydrothermal treatments at 250 ℃ for

90 min (Parr acid digestion bomb, total volume 125 mL) were applied. Obtained Co^{2+} doped TiO_2 nanocrystals were efficiently re-dispersed in water and dialyzed against 10 times larger volume of acidified water (pH = 5) at 4 ℃ for 3 days in order to remove excess of Co^{2+} ions. Water was changed daily. Spectra/Por Dialysis Membrane, MWCO: 3500 (Spetrum Laboratories, Inc., Rancho Dominguez, CA, USA) was used for dialysis.

The percentage ratio of Co^{2+} to Ti^{4+} ions in doped nanocrystals was determined using ICP emission spectrometer (ICAP 6000 series, Thermo Electron Corporation). Prior to the ICP measurements, the powdered sample was dispersed in 3 mL of concentrated sulfuric acid and hydrothermally treated for 60 min at 250 ℃ in Teflon vessel (Parr acid digestion bomb, total volume 25 mL). The final concentrations of Co^{2+} ions in dialyzed samples of doped TiO_2 nanocrystals were 1.69 and 2.5 at% of the amount of Ti^{4+} ions.

The shape and size of precursor titania nanotubes were characterized in Hitachi H-700 FA TEM at 125 kV, while the Co^{2+} doped TiO_2 nanocrystals were characterized by JEOL 100 CX TEM at 100 kV.

Reflectance spectra of powder of Co^{2+} doped TiO_2 nanocrystals were recorded at room temperature using Thermo Scientific Evolution 600 UV/Vis spectrophotometer.

The X-ray diffraction (XRD) patterns were obtained using a Philips PW-1050 automated diffractometer using Cu Kα radiation (operated at 40 kV and 30 mA). Diffraction data for crystallographic analysis were collected in the 2θ range of 10°–120°, with scanning step of 0.02° and exposure time of 12 s. Crystallographic analysis was done using the KOALARIE computing program [28], based on the Rietveld full profile refinement method [29]. Samples for XRD measurements were prepared using standard protocol [30].

The field dependence magnetic moment was measured with a super conducting quantum interference device magnetometer (Quantum Design). The magnetic field was applied parallel to the film surface. The measured magnetization at 300 K was corrected for the diamagnetic background of the glass substrate (derived from high-field dependence magnetization data). Films for magnetic characterization were prepared by drop casting of dialyzed dispersions of Co^{2+} doped TiO_2 nanoparticles onto pre-cleaned glass substrate. The films were annealed in air for 2 min at 100 ℃ after adding each drop. Weights of all films were measured for purposes of determining the amounts of the dopant ions required for magnetic moment calculations.

3 Results and discussion

Titania nanotubes represent a suitable starting material for the synthesis of highly crystalline doped TiO_2 nanoparticles of various sizes and shapes through structural reorganization and shape transformation in the presence of dopant ions. In this study, as precursor were used synthesized titania nanotubes with a layered structure of scrolled nanotubes (Fig. 1(a)). Their size was fairly uniform and with characteristic parameters: outer diameter was in 10 nm range, inner diameter was about 5 nm, while the interlayer spacing was quite large, approximately 0.7 nm (Fig. 1(a)).

Hydrothermal treatment of dispersion of titania nanotubes at pH = 5 in the presence of Co^{2+} ions resulted in formation of Co^{2+} doped TiO_2 nanoparticles (2.5 at% Co^{2+}) of mixed shapes and sizes. The mixture (Fig. 1(b)) consists of polygonal (faceted), non-spherical nanocrystals with average dimension of 14 nm and the larger, anisotropic nanocrystals with shapes like prolate spheroids and lengths up to 120 nm.

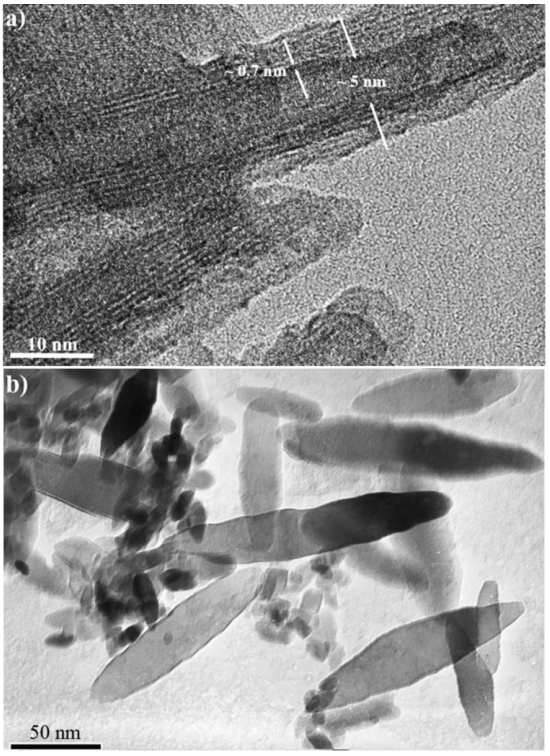

Fig. 1 TEM images of (a) precursor nanotubes and (b) 2.5 at% Co^{2+} doped TiO_2 nanocrystals.

The process of synthesis was controlled by the hydrothermal conditions such as the temperature and duration time as well as the concentration and pH value of precursor dispersions [20,31,32]. Our previous results showed that the hydrothermal treatment of titania nanotubes at pH = 5 leads to formation of elongated, prolate spheroid-like nanocrystals independently of the concentration of starting dispersion of titania nanotubes and the concentration of dopant ions [20]. The appearance of Co^{2+} doped TiO_2 nanoparticles of mixed shapes in this study (Fig. 1(b)), although the synthesis conditions were similar to Ref. [20], can be explained by the modified post-synthetic rinsing procedure of precursor titania nanotubes (rinse once with 1 M HCl, followed by rinsing with H_2O until pH = 7). The release of residual H^+ ions from the interlayers of nanotubes could induce the lowering of the pH during the hydrothermal treatment of nanotubes and hence the appearance of nanocrystals of mixed shapes and sizes.

Barnard and Curtiss [33] used the free energy of nanocrystals as a function of size and shape, to determine the minimum energy morphology of anatase and rutile TiO_2 nanocrystals with different surface chemistry (acid or alkaline conditions). They found that in hydrogen dominancy on the surface (acidic conditions), there is little change in the shape of the nanocrystals with respect to the (neutral) water terminated nanoparticles. However, when oxygen is dominant on the surface (alkaline conditions), the nanoparticles of both polymorphs become elongated. According to Sugimoto and Zhou [34], who studied formation of TiO_2 nanoparticles, their anisotropic growth and increase of the final size, with increasing of pH, are the consequence of the reduction of nucleation rate and increased adsorption of OH^- groups on the embryos of TiO_2 nuclei. By analogy with formation of TiO_2 nanoparticles during dissolution process of $Ti(OH)_4$ gel, the rate-determining step for the growth of doped TiO_2 particles, probably is not the dissolution process of nanotubes than the deposition process of the solute onto the growing TiO_2 particles which proceeds with increasing pH [35]. Under these circumstances, the crystal growth is governed by kinetics, rather than thermodynamics, thus leading to the formation of the metastable anatase [36,37]. Presence of dopant ions can also stabilize anatase crystalline structure of TiO_2 and retard the formation of more stable rutile phase [38].

The XRD pattern of precursor nanotubes is shown in Fig. 2. The development of anatase crystalline phase with characteristic peaks at $2\theta = 25.3°$, 37.9°, 48.2°, 53.9°, 55.1°, and 62.7° assigned to (101), (004), (200), (105), (211), and (204) crystal planes, respectively, was confirmed (JCPDS Card No. 21-1272). Asymmetry of peak which appears at $2\theta = 25.3°$ indicates the presence of monoclinic TiO_2(B) structure ($2\theta = 24.5°$) [39,40] and also hydrogentitanate, compounds which usually appear in the samples of hydrothermally synthesized titania nanotubes. These results follow the trend of observations of the crystal structure of titania nanotubes as quasi-anatase crystal phase with the presence of insignificantly small amount of monoclinic TiO_2(B) crystalline structure [31,41,42].

The XRD analysis of 1.69 and 2.5 at% Co^{2+} doped TiO_2 nanocrystals are presented in Fig. 3. Spectra of the both samples have peaks unambiguously indexed as the tetragonal anatase crystal form of TiO_2. High intensity and sharpness of peaks in the XRD patterns indicate high crystallinity of the samples. No diffraction peaks related to impurities such as metallic Co clusters, CoO, or Co–Ti oxide species are detected, implying incorporation of Co^{2+} ions into TiO_2 crystal lattice. Such finding opens up possibility to correlate magnetic properties to Co^{2+} ions incorporated into anatase lattice.

The crystal parameters of anatase phases in both samples of Co^{2+} doped TiO_2 nanocrystals (1.69 and 2.5 at% Co), based on XRD analysis by Rietveld full profile refinement method, are shown in Table 1. The lattice parameters of the both samples are larger than reference values of the pure anatase (JCPDS Card No. 89-4921) (Table 1). The increase in lattice parameters is a further indication of substitution of Ti^{4+} by Co^{2+} within crystal

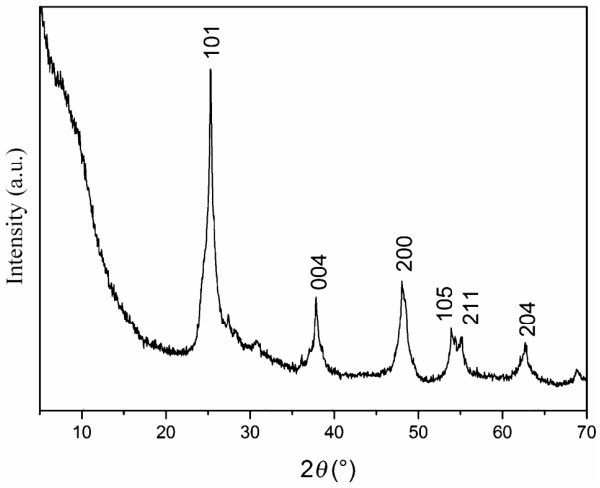

Fig. 2 XRD pattern of precursor nanotubes.

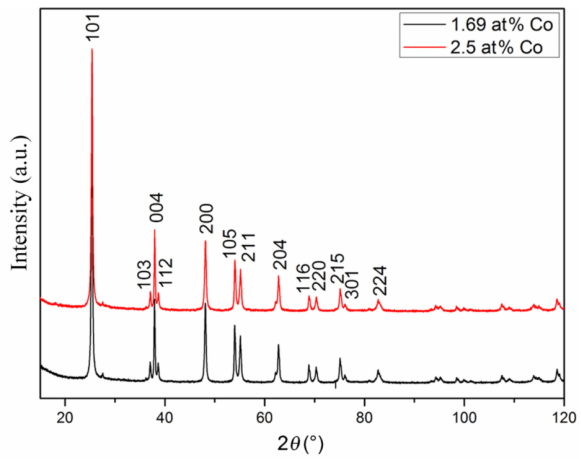

Fig. 3 XRD patterns of 1.69 and 2.5 at% Co^{2+} doped TiO_2 nanocrystals.

Table 1 Refined values of unit cell parameters of Co^{2+} doped TiO_2 nanocrystals

Sample	*a* (Å)	*c* (Å)	*V* (Å^3)
TiO_2	3.77700	9.50100	135.5400
1.69 at% Co	3.78850	9.50816	136.4678
2.5 at% Co	3.78924	9.50791	136.5175

structure of doped TiO_2 nanoparticles [43]. It is known that Co impurities induce local geometrical distortions in crystal lattice of TiO_2 [17]. Ionic radius of Co^{2+} ions in octahedral coordination is 0.79 or 0.885 Å when Co^{2+} is in its high spin state, which is slightly larger than ionic radius of Ti^{4+} ions in octahedral coordination (0.745 Å) [44], while bond lengths with nearest neighboring oxygen surrounding the impurity are reduced by about 0.05 Å [17]. Calculations by Weissmann and Errico [17] predicted that Co^{2+} ions in anatase crystal lattice tend to be located in rows along *a*-axis. Because of the charge imbalance between dopant (Co^{2+}) and host (Ti^{4+}) ions, the overall charge neutrality in the lattice of TiO_2 nanoparticles after incorporation of Co^{2+} ions is maintained by introducing oxygen interstitial defects [3,17]. Due to fact that the TiO_2 is an ionic crystal, formation of oxygen vacancies induces a large structural relaxation as a consequence of the repulsion of nearby titanium ions [3,15,17,45].

In order to further confirm incorporation of Co^{2+} ions into the crystal lattice of TiO_2, we have investigated the optical properties of powdered samples of the 1.69 and 2.5 at% Co^{2+} doped TiO_2 nanoparticles. The reflection spectra of doped TiO_2 nanoparticles are presented in Fig. 4.

The influence of dopant on optical properties of TiO_2 matrix is evident (Fig. 4). Increase of absorbance of

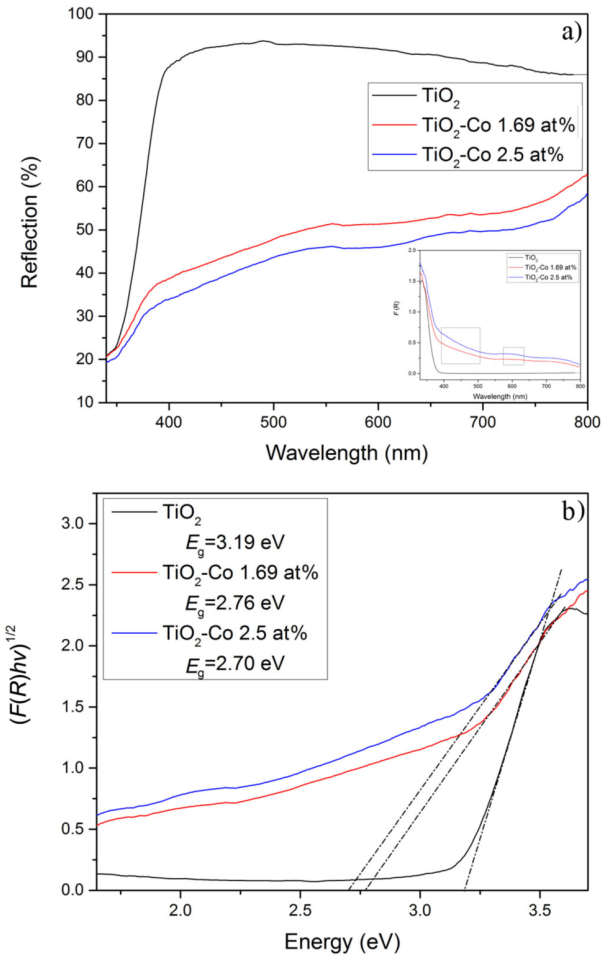

Fig. 4 (a) Reflection spectra of non-doped and 1.69 and 2.5 at% Co^{2+} doped TiO_2 nanocrystals (inset: absorption mode) and (b) band gap determinations.

Co^{2+} doped TiO_2 nanoparticles in the visible part of the spectra could be related to the narrowing of the band gap of TiO_2. As can be seen from Fig. 4(a), there are two specific features observed in the both spectra of Co^{2+} doped TiO_2 nanoparticles: between 400 and 500 nm and around 600 nm. These features are related to the $^4T_{1g}$ to $^4T_{1g}(P)$ and $^4T_{1g}$ to $^4A_{2g}$ transitions, respectively, which are the consequence of crystal field splitting of d-electronic transitions of Co^{2+} in octahedral or pseudo-octahedral coordination [46]. Upon substitution of Ti^{4+} ions by Co^{2+}, the electrons in the d orbital of Co^{2+} will undergo repulsion by the electrons of the six surrounding oxygen atoms which results in the splitting of d orbital of Co^{2+}. Appearance of these transitions in the spectra of doped TiO_2 nanoparticles is an indication of incorporation of Co^{2+} ions in TiO_2 lattice [43,47,48].

For the analysis of reflectance spectra, Kubelka–Munk relation $F(R)=(1-R)^2/2R$, which allows the

optical absorbance ($F(R)$) of the sample to be approximated from its reflectance (R in %), was applied. Using this relation semiconducting materials can be analyzed with a Tauc plot, whereby the absorption coefficient, α, in the Tauc equation is substituted with $F(R)$ ($(F(R)h\nu)^{1/2}=f(h\nu)$, where exponent 1/2 indicates the indirect nature of band-to-band transition) [49,50]. Band gap energies of the Co^{2+} doped TiO_2 nanoparticles synthesized at pH = 5 were estimated from the variation of the Kubelka–Munk function with photon energy (Fig. 4(b)). According to this method, determined band gap energies of 1.69 and 2.5 at% Co^{2+} doped TiO_2 nanocrystals, revealed their red shifts to 2.76 and 2.70 eV, respectively.

While certain groups of authors claimed that doping does not reduce the actual band gap of TiO_2 but instead introduces some mid-band gap states which results in red shift of band gap, other groups associated the narrowing of band gap to the sp–d exchange interactions between the host and dopant ions [51,52]. Owing to formation of oxygen vacancies in the crystal lattice of TiO_2 after substitution of Ti^{4+} with Co^{2+} ions, the defect states in the forbidden zone of the energy band gap of TiO_2 are created. The existence of these defect states is a reason for appearance of absorption bands in the visible spectral region [53]. Some theoretical calculations suggested that a high vacancy concentration could induce a vacancy band of electronic states just below the conduction band [54]. According to Zuo *et al*. [55], the band gap narrowing in Co^{2+} doped TiO_2 nanoparticles is a consequence of the presence of a mini-band just below the conduction band minimum, related to the oxygen vacancy associated with Ti^{3+}.

The magnetic responses of films in dependence of magnetic field are shown in Fig. 5. Weak ferromagnetic behavior was observed in both samples, with coercive field of $H_c \approx 100$ Oe and low saturation moments in the range of $M_s = 0.001 - 0.002$ μ_B/Co. The diamagnetic contribution determined from the room temperature magnetic field dependence of magnetization at high field (for $H > 10$ kOe) was subtracted in both samples and not considered below. According to saturation magnetization values, the total number of magnetic moments in Co^{2+} doped TiO_2 nanoparticles increases with increasing amount of dopant ions (Fig. 5).

Furthermore, temperature dependence of magnetic susceptibility ($H = 1000$ Oe) in films made of 1.69 and 2.5 at% Co^{2+} doped TiO_2 nanocrystals enabled the

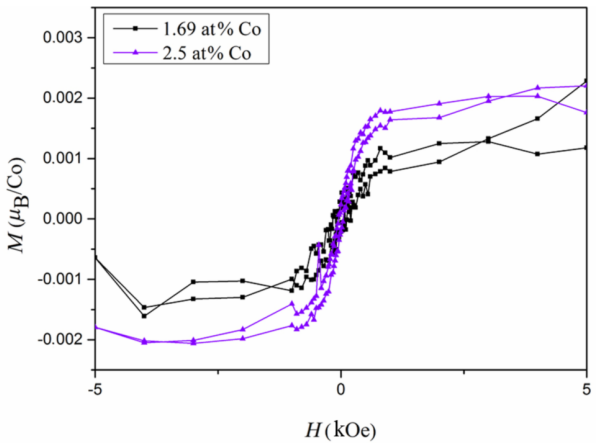

Fig. 5 Room temperature magnetizations of the films made of 1.69 and 2.5 at% Co^{2+} doped TiO_2 nanocrystals.

examination of the nature of magnetism (Fig. 6). The increase of susceptibility is observed at low temperature for both samples indicating dominant paramagnetic behavior of isolated Co^{2+} ions [56]. Zero-field-cooled (ZFC) and field-cooled (FC) magnetic susceptibility (not shown) under low field of 100 Oe completely overlap for both samples showing no change from behavior presented in Fig. 6, without signature of Co magnetic clusters. Temperature dependent susceptibility follows Curie–Weiss's dependence:

$$\chi = \frac{C}{T-\theta} \tag{1}$$

where C is Curie constant and θ is Curie–Weiss temperature, indicating the straight nature of the magnetic interactions. The values of C and θ obtained from the fit of Curie–Weiss law are given in Table 2.

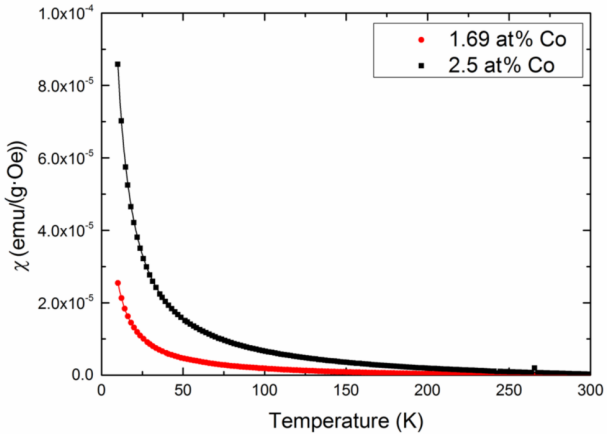

Fig. 6 Temperature variations of the magnetic susceptibility measured at H=1000 Oe. Solid lines represent Curie–Weiss fit.

Table 2 Values of C, θ, and μ_{eff} obtained from Curie–Weiss fit for 1.69 and 2.5 at% Co^{2+} doped TiO_2

Sample	C (emu·K/(g·Oe))	θ (K)	μ_{eff} (μ_B/Co)
1.69 at% Co	2.99×10^{-4}	1.2	3.4
2.5 at% Co	6.51×10^{-4}	0.2	4.1

In both samples, θ has a very small positive value indicating very weak ferromagnetic coupling. The Curie constant, C, is related to the effective magnetic moment μ_{eff} of Co^{2+} in Co^{2+} doped TiO_2 through the relation [57]:

$$C = \frac{N\mu_{eff}^2\mu_B^2}{3k_B} \quad (2)$$

where N is the number of interaction magnetic ions per g, μ_B is Bohr magneton, and k_B is Boltzmann constant. The effective magnetic moment calculated from the experimental values of Curie constant, Table 2, are very close to the theoretical value (μ_{eff} = 3.87 μ_B/Co) for high-spin (S=3/2) Co^{2+} with the quenching of orbital angular moment under the crystal field formed by surrounding O^{2-} ions [58]. The magnitude of experimentally estimated μ_{eff} indicates that high-spin Co^{2+} ions contribute to the paramagnetic behavior of the Co^{2+} doped TiO_2 films, as well as to the ferromagnetic behavior observed at room temperature (Fig. 5). The oxygen defects/vacancies surrounding Co^{2+} ions appear to be crucial parameter leading to weak ferromagnetic behavior.

In general, ferromagnetic ordering in transition metal doped TiO_2 could be explained in terms of the non-carrier mediated bound magnetic polaron (BMP) model. According to this theory, when defect concentration exceeds the percolation threshold, oxygen vacancy defects overlap many dopant ions to yield BMPs, which results in ferromagnetic coupling between dopant ions mediating through oxygen vacancy [8,14]. The polaron percolation threshold, δ_p, and the dopant cation percolation threshold, x_p, represent two main parameters that determine the nature of the magnetic interaction. Ferromagnetic ordering occurs when $\delta > \delta_p$ and $x < x_p$, while antiferromagnetism or ferrimagnetism appears beyond x_p, where there are continuous paths throughout the crystal, joining nearest-neighbor magnetic cations [14]. Slight increase of the value of magnetic moment with increasing the concentration of Co^{2+} ions in studied samples (Fig. 5), indicated that the dopant concentration does not exceed the percolation threshold.

On the other hand, a significant decrease of magnetic moment per cobalt atom was observed in 1.69 and 2.5 at% Co^{2+} doped TiO_2 nanocrystals of various shapes (polygonal and prolate spheroids), compared to the magnetic moment per Co (0.25 μ_B/Co) reported in our previous work, for 0.46 at% Co^{2+} doped TiO_2 nanocrystals (only polygonal), synthesized in the same way [24]. According to literature, there are several reasons for the observed reduction of the magnetic moment per cation. The possible existence of clusters of antiferromagnetically-coupled spins when dopant cation concentration is less than dopant cation percolation threshold ($x < x_p$), can reduce the average moment per cation [14]. However, obtained magnetization curves with observed saturation (Fig. 5), indicate no such paraprocess involved. Also, the existence of low-spin state of Co^{2+} is excluded if it is incorporated in anatase TiO_2 [59]. Yermakov *et al*. [60] explained observed reduction of the magnetic moment in nanocrystalline TiO_2:Co samples by itinerant magnetism model due to cobalt localization and magnetic ordering on the surface which also contains oxygen defects.

It is known that the concentration of oxygen vacancies, i.e., undercoordinated defects in TiO_2 nanocrystals depends on their surface morphologies and sizes [42]. A low concentration of oxygen vacancies in 1.69 and 2.5 at% Co^{2+} doped TiO_2 nanocrystals could be the reason for the observed significantly lower magnetic moment in spite of relatively high concentrations of dopant ions (max. 2.5 at%) in comparison to 0.46 at% Co^{2+} doped TiO_2 nanoparticles [24]. Since TEM characterization (Fig. 1(b)) revealed mixture of finer polygonal and coarser prolate ellipsoid nanocrystals in 2.5 at% Co^{2+} doped TiO_2 sample, the low value of magnetic moment in this sample might be related to lower level of surface oxygen vacancy defects in prolate nanospheroids [61]. To confirm the existence of different concentration of oxygen vacancies in polygonal and prolate ellipsoid TiO_2 nanocrystals, we applied photoluminescence spectroscopy, a method sensitive to the presence of defects in the crystalline structure of semiconductor nanoparticles [21]. Photoluminescence spectrum of TiO_2 nanocrystals of different shapes (polygonal and prolate spheroids) after band gap excitation at λ_{exc}=365 nm which were synthesized under the same experimental conditions but in absence of Co ions is shown in Fig. 7.

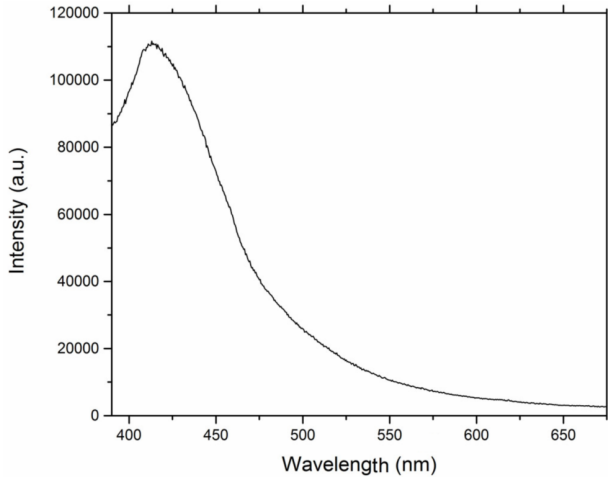

Fig. 7 PL spectrum of non-doped TiO_2 nanocrystals of mixed shapes (polygonal and prolate ellipsoid).

An intense band observed at 2.95 eV (420 nm) can be assigned to the lowest indirect transition from the center to the edge of the Brillouin zone, Γ_{1b}–X_{1a} [62]. Absence of intense bands in the low energy region of PL spectrum was an indication of lower concentration/amount of structural defects. Namely, in our previous work we reported that appearance of the lower energy emissions in the photoluminescence spectrum of polygonal (only) TiO_2 nanocrystals, at 2.88 and 2.56 eV, which originate from the intra-gap levels transitions, was an indication of existence of lattice and/or surface structural defects (oxygen vacancies) [21]. Observed difference in PL spectrum of TiO_2 nanocrystals consisting of polygonal and prolate spheroid-like particles (Fig. 7), compared to only polygonal TiO_2 particles [21] implied to the significantly lower concentration of oxygen vacancies in prolate spheroid-like nanocrystals. Such assumption is in agreement with their larger dimension, decreased curvature, and consequently lower amount of surface defects. Finally, it can be concluded that room temperature ferromagnetism observed in our sample is directly correlated to the concentration of oxygen vacancies.

However, Santara *et al*. [63] demonstrated that concentration of oxygen vacancies by itself does not affect the magnitude of magnetic moment, but they also suggested that the defect environment and the surface morphology of the nanoparticles could be of crucial importance for achieving of measurable ferromagnetic interaction. The greater density of the oxygen vacancy helps to produce more BMP which yields a greater overall volume occupied by BMP, leading to an overlap of BMPs and enhancing ferromagnetic behavior.

4 Conclusions

In summary, Co^{2+} doped TiO_2 nanocrystals were synthesized in a two-step hydrothermal method. Dispersions of previously synthesized titania nanotubes in the presence of different concentrations of Co^{2+} ions at pH = 5, were used as precursors. XRD study demonstrated the absence of impurity phases and confirmed anatase crystal structure in 1.69 and 2.5 at% Co^{2+} doped TiO_2 nanocrystals independently of the concentrations of dopant ions. TEM analysis revealed the presence of the mixture of polygonal nanocrystals, with average dimension of 14 nm, and prolate spheroid-like nanocrystals with lengths up to 120 nm. Both samples of 1.69 and 2.5 at% Co^{2+} doped TiO_2 nanocrystals exhibited weak ferromagnetic ordering with closed loop and coercivity $H_c \approx 100$ Oe, accompanied with paramagnetic behavior. The low values of magnetic moments per Co in both samples that contain polygonal and prolate spheroid-like nanocrystals, were probably the consequence of the lower total number of surface defects/oxygen vacancies. The PL spectrum of non-doped TiO_2 nanocrystals of different shapes confirmed the lower number of surface defects (oxygen vacancies) within.

Acknowledgements

The financial support for this work was provided by the Ministry of Education, Science and Technological Development of Republic of Serbia (Project Nos. OI 172056 and III 45020). This work was done under umbrella of COST Action MP1106. Z. K. thanks for the support from the project III 45018 from the Ministry of Education, Science and Technological Development of Republic of Serbia. TEM characterization of titania nanotubes was provided by Prof. P. Ahrenkiel, South Dakota School of Mines & Technology, Rapid City, SD, USA.

References

[1] Janisch R, Gopal P, Spaldin NA. Transition metal-doped TiO_2 and ZnO—Present status of the field. *J Phys: Condens Matter* 2005, **17**: R657–R689.

[2] Nguyen HH, Prellier W, Sakai J, *et al*. Substrate effects on the room-temperature ferromagnetism in Co-doped TiO_2 thin films grown by pulsed laser deposition. *J Appl Phys* 2004, **95**: 7378–7380.

[3] Kim J-Y, Park J-H, Park B-G, *et al*. Ferromagnetism

induced by clustered Co in Co-doped anatase TiO_2 thin films. *Phys Rev Lett* 2003, **90**: 017401.

[4] Kennedy RJ, Stampe PA, Hu E, *et al*. Hopping transport in TiO_2:Co: A signature of multiphase behavior. *Appl Phys Lett* 2004, **84**: 2832–2834.

[5] Hong NH, Sakai J, Prellier W. Distribution of dopant in Fe:TiO_2 and Ni:TiO_2 thin films. *J Magn Magn Mater* 2004, **281**: 347–352.

[6] Sharma P, Gupta A, Rao KV, *et al*. Ferromagnetism above room temperature in bulk and transparent thin films of Mn-doped ZnO. *Nat Mater* 2003, **2**: 673–677.

[7] Lim S-W, Jeong M-C, Ham M-H, *et al*. Hole-mediated ferromagnetic properties in $Zn_{1-x}Mn_xO$ thin films. *Jpn J Appl Phys* 2004, **43**: L280–L283.

[8] Patel SKS, Gajbhiye NS. Room temperature magnetic properties of Cu-doped titanate, TiO_2(B) and anatase nanorods synthesized by hydrothermal method. *Mater Chem Phys* 2012, **132**: 175–179.

[9] Venkatesan M, Fitzgerald CB, Lunney JG, *et al*. Anisotropic ferromagnetism in substituted zinc oxide. *Phys Rev Lett* 2004, **93**: 177206.

[10] Yan L, Ong CK, Rao XS. Magnetic order in Co-doped and (Mn,Co) codoped ZnO thin films by pulsed laser deposition. *J App Phys* 2004, **96**: 508–511.

[11] Gupta A, Cao H, Parekh K, *et al*. Room temperature ferromagnetism in transition metal (V, Cr, Ti) doped In_2O_3. *J Appl Phys* 2007, **101**: 09N513.

[12] Wang XL, Dai ZX, Zeng Z. Search for ferromagnetism in SnO_2 doped with transition metals (V, Mn, Fe, and Co). *J Phys: Condens Matter* 2008, **20**: 045214.

[13] Ogale SB. Dilute doping, defects, and ferromagnetism in metal oxide systems. *Adv Mater* 2010, **22**: 3125–3155.

[14] Coey JMD, Venkatesan M, Fitzgerald CB. Donor impurity band exchange in dilute ferromagnetic oxides. *Nat Mater* 2005, **4**: 173–179.

[15] Errico LA, Rentería M, Weissman M. Theoretical study of magnetism in transition-metal-doped TiO_2 and $TiO_{2-\delta}$. *Phys Rev B* 2005, **72**: 184425.

[16] Choudhury B, Choudhury A. Oxygen vacancy and dopant concentration dependent magnetic properties of Mn doped TiO_2 nanoparticle. *Curr Appl Phys* 2013, **13**: 1025–1031.

[17] Weissmann M, Errico LA. The role of vacancies, impurities and crystal structure in the magnetic properties of TiO_2. *Physica B* 2007, **398**: 179–183.

[18] Erwin SC, Zu L, Haftel MI, *et al*. Doping semiconductor nanocrystals. *Nature* 2005, **436**: 91–94.

[19] Bryan JD, Gamelin DR. Doped semiconductor nanocrystals: Synthesis, characterization, physical properties, and applications. *Prog Inorg Chem* 2005, **54**: 47–126.

[20] Vranješ M, Kuljanin-Jakovljević J, Radetić T, *et al*. Structure and luminescence properties of Eu^{3+} doped TiO_2 nanocrystals and prolate nanospheroids synthesized by the hydrothermal processing. *Ceram Int* 2012, **38**: 5629–5636.

[21] Vranješ M, Kuljanin-Jakovljević J, Ahrenkiel SP, *et al*. Sm^{3+} doped TiO_2 nanoparticles synthesized from nanotubular precursors—Luminescent and structural properties. *J Lumin* 2013, **143**: 453–458.

[22] Vranješ M, Konstatinović Z, Pomar A, *et al*. Room-temperature ferromagnetism in Ni^{2+} doped TiO_2 nanocrystals synthesized from nanotubular precursors. *J Alloys Compd* 2014, **589**: 42–47.

[23] Vranješ M, Kuljanin-Jakovljević J, Konstatinović Z, *et al*. Room temperature ferromagnetism in Cu^{2+} doped TiO_2 nanocrystals: The impact of their size, shape and dopant concentration. *Mater Res Bull* 2016, **76**: 100–106.

[24] Kuljanin-Jakovljević J, Radoičić M, Radetić T, *et al*. Presence of room temperature ferromagnetism in Co^{2+} doped TiO_2 nanoparticles synthesized through shape transformation. *J Phys Chem C* 2009, **113**: 21029–21033.

[25] Yan HG, Zeng HC. Synthetic architectures of $TiO_2/H_2Ti_5O_{11}\cdot H_2O$, $ZnO/H_2Ti_5O_{11}\cdot H_2O$, $ZnO/TiO_2/H_2Ti_5O_{11}\cdot H_2O$, and ZnO/TiO_2 nanocomposites. *J Am Chem Soc* 2005, **127**: 270–278.

[26] Yang X, Karthik C, Li X, *et al*. Oriented nanocrystal arrays of selectable polymorphs by chemical sculpture. *Chem Mater* 2009, **21**: 3197–3201.

[27] Kasuga T, Hiramatsu M, Hoson A, *et al*. Titania nanotubes prepared by chemical processing. *Adv Mater* 1999, **11**: 1307–1311.

[28] Cheary RW, Coelho A. A fundamental parameters approach to X-ray line-profile fitting. *J Appl Cryst* 1992, **25**: 109–121.

[29] Rietveld HM. A profile refinement method for nuclear and magnetic structures. *J Appl Cryst* 1969, **2**: 65–71.

[30] Pecharsky VK, Zavalij PY. *Fundamentals of Powder Diffraction and Structural Characterization of Materials*. New York: Springer, 2009.

[31] Šaponjić ZV, Dimitrijević NM, Poluektov OG, *et al*. Charge separation and surface reconstruction: A Mn^{2+} doping study. *J Phys Chem B* 2006, **110**: 25441–25450.

[32] Dimitrijević NM, Šaponjić ZV, Rabatić BM, *et al*. Effect of size and shape of nanocrystalline TiO_2 on photogenerated charges. An EPR study. *J Phys Chem C* 2007, **111**: 14597–14601.

[33] Barnard AS, Curtiss LA. Prediction of TiO_2 nanoparticle phase and shape transitions controlled by surface chemistry. *Nano Lett* 2005, **5**: 1261–1266.

[34] Sugimoto T, Zhou X. Synthesis of uniform anatase TiO_2 nanoparticles by the gel–sol method: 2. Adsorption of OH^- ions to $Ti(OH)_4$ gel and TiO_2 particles. *J Colloid Interface Sci* 2002, **252**: 347–353.

[35] Sugimoto T, Zhou X, Muramatsu A. Synthesis of uniform anatase TiO_2 nanoparticles by gel–sol method: 1. Solution chemistry of $Ti(OH)_n^{(4-n)+}$ complexes. *J Colloid Interface Sci* 2002, **252**: 339–346.

[36] Nian J-N, Teng H. Hydrothermal synthesis of single-crystalline anatase TiO_2 nanorods with nanotubes as the precursor. *J Phys Chem B* 2006, **110**: 4193–4198.

[37] Bischoff BL, Anderson MA. Peptization properties in the sol–gel preparation of porous anatase (TiO_2). *Chem Mater* 1995, **7**: 1772–1778.

[38] De los Santos DM, Navas J, Sánchez-Coronilla A, *et al*. Highly Al-doped TiO_2 nanoparticles produced by ball mill method: Structural and electronic characterization. *Mater Res Bull* 2015, **70**: 704–711.

[39] Delgado AV, González-Caballero F, Hunter RJ, *et al*. Measurement and interpretation of electrokinetic phenomena. *J Colloid Interface Sci* 2007, **309**: 194–224.
[40] Yahia MB, Lemoigno F, Beuvier T, *et al*. Updated references for the structural, electronic, and vibrational properties of TiO_2(*B*) bulk using first-principles density functional theory calculations. *J Chem Phys* 2009, **130**: 204501.
[41] Vranješ M, Šaponjić ZV, Živković LS, *et al*. Elongated titania nanostructures as efficient photocatalysts fordegradation of selected herbicides. *Appl Catal B: Environ* 2014, **160–161**: 589–596.
[42] Šaponjić ZV, Dimitrijević NM, Tiede DM, *et al*. Shaping nanometer-scale architecture through surface chemistry. *Adv Mater* 2005, **17**: 965–971.
[43] Khurana C, Pandey OP, Chudasama B. Synthesis of visible light-responsive cobalt-doped TiO_2 nanoparticles with tunable optical band gap. *J Sol–Gel Sci Technol* 2015, **75**: 424–435.
[44] Cobalt: Radii of atoms and ions. Available at http://www.webelements.com/cobalt/atom_sizes.html.
[45] You M, Kim TG, Sung Y-M. Synthesis of Cu-doped TiO_2 nanorods with various aspect ratios and dopant concentracion. *Cryst Growth Des* 2010, **10**: 983–987.
[46] Lee JD. *Concise Inorganic Chemistry*. John Wiley & Sons, 2008.
[47] Choudhury B, Choudhury A. Luminescence characteristics of cobalt doped TiO_2 nanoparticles. *J Lumin* 2012, **132**: 178–184.
[48] Husain S, Alkhtaby LA, Giorgetti E, *et al*. Influence of cobalt doping on the structural, optical and luminescence properties of sol–gel derived TiO_2 nanoparticles. *Philos Mag A* 2017, **97**: 17–27.
[49] Tauc J, Grigorovici R, Vancu A. Optical properties and electronic structure of amorphous germanium. *Phys Status Solidi b* 1966, **15**: 627–637.
[50] Pal M, Pal U, Jimenez JMGY, *et al*. Effects of crystallization and dopant concentration on the emission behavior of TiO_2:Eu nanophosphors. *Nanoscale Res Lett* 2012, **7**: 1–12.
[51] Das K, Sharma SN, Kumar M, *et al*. Morphology dependent luminescence properties of Co doped TiO_2 nanostructures. *J Phys Chem C* 2009, **113**: 14783–14792.
[52] Archer PI, Santangelo SA, Gamelin DR. Direct observation of sp-d exchange interactions in colloidal Mn^{2+}- and Co^{2+}-doped CdSe quantum dots. *Nano Lett* 2007, **7**: 1037–1043.
[53] Emeline AV, Kuznetsov VN, Rybchuk VK, *et al*. Visible-light-active titania photocatalysts: The case of N-doped TiO_2s—Properties and some fundamental issues. *International Journal of Photoenergy* 2008, **2008**: Article ID 258394.
[54] Justicia I, Ordejon P, Canto G, *et al*. Designed self-doped titanium oxide thin films for efficient visible-light photocatalysis. *Adv Mater* 2002, **14**: 1399–1402.
[55] Zuo F, Wang L, Wu T, *et al*. Self-doped Ti^{3+} enhanced photocatalyst for hydrogen production under visible light. *J Am Chem Soc* 2010, **132**: 11856–11857.
[56] Anitha B, Abdul Khadar A, Banerjee A. Paramagnetic behavior of Co doped TiO_2 nanocrystals controlled by self-purification mechanism. *J Solid State Chem* 2016, **239**: 237–245.
[57] Punnoose A, Hays J, Shutthanandan V, *et al*. Room-temperature ferromagnetism in chemically synthesized $Sn_{1-x}Co_xO_2$ powders. *Appl Phys Lett* 2004, **85**: 1559.
[58] Spaldin NA. *Magnetic Materials: Fundamentals and Applications*. Cambridge University Press, 2003.
[59] Geng WT, Kim KS. Interplay of local structure and magnetism in Co-doped TiO_2 anatase. *Solid State Commun* 2004, **129**: 741−746.
[60] Yermakov AY, Zakharova GS, Uimin MA, *et al*. Surface magnetism of cobalt-doped anatase TiO_2 nanopowders. *J Phys Chem C* 2016, **120**: 28857−28866.
[61] Rabatic BM, Dimitrijevic NM, Cook RE, *et al*. Spatially confined corner defects induce chemical functionality of TiO_2 nanorods. *Adv Mater* 2006, **18**: 1033−1037.
[62] Daude N, Gout C, Jouanin C. Electronic band structure of titanium dioxide. *Phys Rev B* 1977, **15**: 3229.
[63] Santara B, Giri PK, Imakita K, *et al*. Evidence of oxygen vacancy induced room temperature ferromagnetism in solvothermally synthesized undoped TiO_2 nanoribbons. *Nanoscale* 2013, **5**: 5476−5488.